The solar spectral irradiance as a function of the Mg II index for atmosphere and climate modelling

Gérard Thuillier[1], Matthew DeLand[2], Alexander Shapiro[3],
Werner Schmutz[3], David Bolsée[4], Stella Melo[5]

[1] LATMOS-CNRS 11 boulevard d'Alembert, 78280 Guyancourt, France
[2] SSAI, 10210 Greenbelt Road, Suite 600, Lanham, MD 20706 USA
[3] PMOD-WRC Dorfstrasse 33, Davos, CH-7260, Switzerland
[4] Solar-Terrestrial Centre of Excellence - BIRA-IASB, 3 avenue Circulaire, B1180 Bruxelles, Belgique
[5] Canadian Space Agency, 6767 route de l'Aéroport, Saint-Hubert, Québec, Canada

Abstract

In this paper we present a new method to reconstruct the solar spectrum irradiance in the Ly α-400 nm region, and its variability, based on the Mg II index and neutron monitor. Measurements of the solar spectral irradiance available in the literature have been made with different instruments at different times and different spectral ranges. However, climate studies require harmonized data sets.
This new approach has the advantage of being independent of the absolute calibration and aging of the instruments. First, the Mg II index is derived using solar spectra from Ly α (121 nm) to 410 nm measured from 1978 to 2010 by several space missions. The variability of the spectra with respect to a chosen reference spectrum as a function of time and wavelength is scaled to the derived Mg II index. The set of coefficients expressing the spectral variability can be applied to the chosen reference spectrum to reconstruct the solar spectra within a given time frame or Mg II index values. The accuracy of this method is estimated using two approaches: by direct comparison with particular cases where solar spectra are available from independent measurements, and by calculating the standard deviation between the measured spectra and their reconstruction. From direct comparisons with measurements we obtain an accuracy of about 1 to 2 %, which degrades towards Ly α. In a further step, we extend our solar spectral irradiance reconstruction back to the Maunder Minimum introducing the relationship between the Mg II index and the neutron monitor data. Consistent measurements of the Mg II index are not available prior to 1978. However, we observe that over the last three solar cycles, the Mg II index shows strong correlation with the modulation potential determined from the neutron monitor data. Assuming that this correlation can be applied to the past, we reconstruct the Mg II index from the modulation potential back to the Maunder Minimum, and obtain the corresponding solar spectral irradiance reconstruction back to that period. As there is no direct measurement of the spectral irradiance for this period we discuss this methodology in light of the other proposed approaches available in the literature.
The use of the cosmogenic isotope data provides a major advantage: it provides information about the solar activity over several thousands years. Using technology of today we can calibrate the solar irradiance against the activity and thus reconstruct it for the times when cosmogenic isotope data are available. This calibration can be re-accessed at any time, if necessary.

1. Introduction

1.1 Atmosphere and climate modelling

The thermal structure, the composition, and the dynamics of the Earth's atmosphere are a consequence of the solar spectral irradiance, by means of the processes of photodissociation, photoionisation, thermal absorption, and photoabsorption. All these processes are implemented in a more or less sophisticated way in most of the climate models to understand the relative roles of the solar activity and greenhouse gas increase:

The 0.75°C warming in the global average surface temperature observed over the second half of last century is largely attributed to anthropological increase in greenhouse gases (Austin et al., 2008). While the anthropogenic forcing acts as an amplifying factor, the underlying climate is defined by the natural drivers. Therefore, realistic modelling of climate scenarios requires the inclusion of variable solar input. The thermal balance and the composition of the atmosphere respond to changes in both the total solar irradiance (TSI) and the spectral solar irradiance (SSI). While the troposphere is directly forced by changes in the TSI, the stratospheric response has a strong dependency on the spectral distribution of the irradiance (Semeniuk et al., 2010, Haigh et al, 2010). The coupling between the stratosphere and the troposphere makes it important to properly model both atmospheric regions. For example, recent analysis by Solomon et al. (2010) has shown that changes in the stratospheric water vapour can in fact affect the surface temperature and offset or amplify the heating due to changes in anthropogenic greenhouse gases. The inclusion of variable solar forcing in numerical climate and atmospheric models requires harmonized and consistent series of TSI and SSI over the time scale of analysis. Furthermore, given the relatively small magnitude of the response obtained with current models (see for example Austin et al., 2008 and the references therein) and the sensitivity of this response to the uncertainties affecting the adopted SSI values (Shapiro et al., 2011b), it is important that the harmonization of existent data sets does not amplify the measurement uncertainties.

Numerical climate modelling, if sophisticated enough to allow for variable SSI forcing, would require the solar spectral irradiance as input. The model performance has to be validated and for that model simulations can be tested against measurements. For example, model estimation of concentration of minor components may be compared to measured quantities. However, the solar signal in the model is relatively small and can be comparable to the model internal variability. To overcome this difficulty, model experiments includes several runs preferably over several solar cycles. Furthermore, to study processes associated to different level of solar variability and different anthropogenic effects we may choose to run the models in periods such as the Maunder Minimum. This leads to the need of past reconstructions of the SSI.

Climate simulations at the scale of millennium can be performed for different scenarios including different solar conditions, greenhouse gas (GHG) concentration, and dust from volcanic activity. For example, the last millennium has the following forcings:

- Nearly constant GHG concentration up to 1800,
- The Medieval Maximum, with high solar activity, constant GHG, and volcanism,
- The Maunder Minimum time frame (1645-1710) with a very low but nearly constant solar activity, but with some periods of significant volcanic activity,
- The Dalton Minimum period, which experienced a rapid climate change,
- The XIX^{e} century with volcanism, solar activity change and increasing GHG concentration,
- The XX^{e} century with limited volcanic activity, but solar activity change, and increasing GHG concentration.

Solar measurements encompassing the entire last millennium are not available. Therefore, reconstructions are required. Even in the case of the first part of the XX^{e} century, no accurate solar spectrum is available. The use of solar proxies becomes a must.

Proxies are quantities that are expected to reproduce the solar variability and its main manifestations, such as its total and spectral irradiance, with a certain accuracy. Several proxies exist such as the Mg II and Ca II core to wing ratio, the solar decimetric flux (F10.7), the He II (1083 nm) line intensity, the photographs taken at the Greenwich observatory since 1874, the sunspot number registered since 1609, the cosmogenic isotopes ^{10}Be and ^{14}C available back to 7000 BC, and even before, but with lower accuracy.

Several proxies being now available, the past solar spectral irradiance is reconstructed using different proxies and methods. Lean (2000) has generated daily spectral irradiances since 1882 ranging from 100 nm to 100 μm, using proxy indices for facular brightening and sunspot darkening. Egorova et al. (2008) produced reconstructed spectral irradiances in the wavelength range 120-680 nm, using irradiance data at Ly α and the Herzberg continuum (200-220 nm) measured by the LYRA instrument on the ESA PROBA-2 satellite. Krivova et al. (2009) uses the evolution of the solar surface magnetic field as a UV proxy and relates magnetogram data to the 220-240 nm spectral irradiance measured by the SUSIM spectrometer on board the Upper Atmosphere Research Satellite (UARS), then uses a linear regression to extend this relationship to the wavelength range 115-410 nm. Bolduc et al. (2011) use photographs from the Greenwich Observatory to reconstruct the solar spectral irradiance since 1874. This reconstruction relies on a three-component model (quiet sun, spots and faculae/network) of spectral irradiance, with a data-driven Monte Carlo simulation of the emergence and decay of solar active regions providing the time-varying surface coverage of the three structure classes.

In this article, we exploit the relationship between the Mg II index and the modulation potential obtained from the ^{10}Be data (McCracken et al. 2004) as being both linked to the solar activity. The advantage of this new approach is to reconstruct the solar spectral variability using measurements without the need of absolute values. It is done by using the modulation potential together with the Mg II index, which is insensitive to the instrument aging, and a single reference spectrum, which can be a given measured spectrum or be calculated from solar models.

1.2 The adoption of the Mg II index

Long series of solar indices are important and useful for many applications including solar and climate modelling. Among the existing solar indices, a choice has to be made. The present work requires a solar index which best represents the SSI variability in the 120-400 nm wavelength domain, i. e. the photospheric and chromospheric emissions; extends over a large time interval; and the least dependent of the measurement conditions, i. e. elements like the atmospheric conditions.

The decimetric flux (F10.7) has been measured since 1947 in Canada (Tapping, 1987). However, it represents a mixture of thermal emission from the solar transition region and contribution from solar magnetic regions. Therefore, it is most suitable to represent the EUV part of the SSI variability. Sunspots and facula number are more relevant for TSI modelling than SSI given their involvement in surface brightness. There are a few approaches which are using the sunspots and the filling factors of other active regions to reconstruct the SSI. This approach needs a detailed analysis of the disk images (which are only available after 1874).

The advantage of the Mg II approach is that we basically need only one number to reconstruct SSI variability.

The Ca II index is defined as the core to wing intensity ratio. Since chromospheric lines are present in the core, its magnitude depends on solar activity. Since the emission rate of the EUV and UV solar lines is linked to the structure of the solar magnetic field, the extent and brightness of the Ca II plages have been considered as proxies for that spectral domain (Lean et al., 1982; White et al., 1992; Neupert, 1998). Consequently, it is well accepted that regular measurements of the Ca II index would constitute a very useful proxy. However, even today the Ca II series of measurements suffers from frequent gaps and the atmospheric noise which limit the utilization of the CaII index for reconstructions that cover for long temporal periods.

The Mg II index was first proposed by Heath and Schlesinger (1986). We use here the Mg II definition given by Cebula and DeLand (1998) obtained by calculating the ratio between the core emission and the solar continuum (referred as the wings) as shown in Figure 1b. In the core of the absorption Mg II Fraunhofer line at 280 nm, the H and K components are observable as calculated (Figure 1a) by the COde for Solar Irradiance (COSI) (Haberreiter et al., 2008, Shapiro et al. 2010). The Mg II line structure at high resolution shows a large number of lines which are smoothed out by the low resolution of the instruments used for the measurements (Figure 1b). Consequently, the Mg II index depends on their slit function and is instrument dependent. However, Mg II index values from different instruments scale depend in a very linear manner, which makes it possible to transform all measurements to a single reference scale. As it does not require the instrument to work in the absolute scale, this index has the advantage of being quasi independent of the instrument degradation. It is only measurable from space given the total absorption by the Earth's atmosphere below 295 nm. Given that the space missions measuring the Mg II line overlap, a unique time series has been established, spanning from 1978 to 2010 (Viereck et al., 2004).

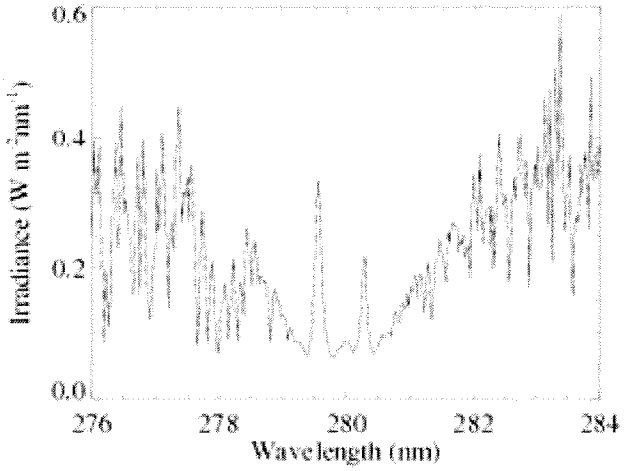

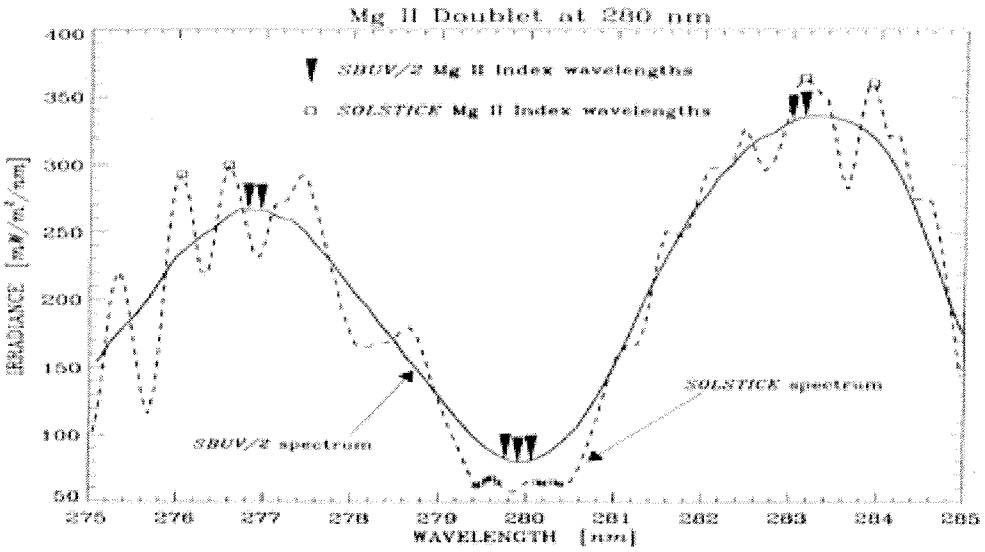

Figure 1: *a*, (upper panel) The Mg II line at high resolution calculated by the COSI model. *b*, (lower panel) The Mg II line observed by a spectrometer at low resolution showing how the Mg II index is calculated based on the core to wing ratio (Cebula et al., 1992). The Mg II doublet is shown by different instrument, SBUV/2 on board NOAA 11, and SOLSTICE on board UARS, at 1.1 and 0.24 nm resolution, respectively.

Avrett (1992) showed, from a theoretical study, that the thermal emission contribution to F 10.7 emission originates at the transition region, while the Mg II and Ca II emission lines originate at nearly the same altitude in the high photosphere for the wings, and high chromosphere for the core. Consequently, both indices behave similarly and correlate with each other (0.975), as shown by Donnelly et al. (1994). In Figure 2 we present the wavelength dependence on height (and therefore on the solar region) calculated with COSI of the formation height in the cores of the strong lines and in the continuum and wings of these lines. For example one can see that the core of Mg II line is formed around 2000 km, while the wings are formed around 300 km. Consequently, we understand why the Mg II index describes the UV emission variability down to the Ly α (121.6 nm) emission (Lean et al., 1992*)*

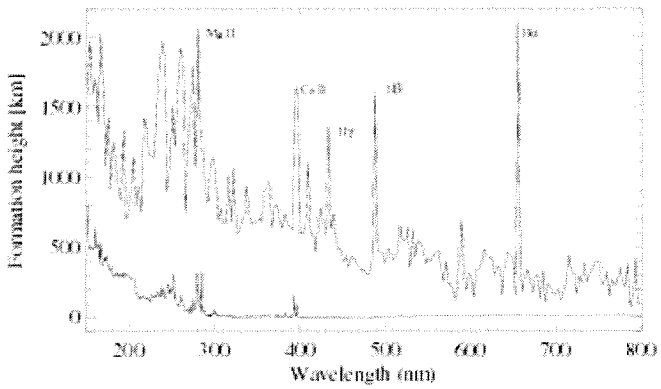

Figure 2: The formation height in the core of the strongest lines (upper curve) and a minimal formation height in a 0.5 nm interval (lower curve), which comes close to what could be called pseudo continuum.

2. Modeling the spectral irradiance for 1978-2010

2.1 The data used in this work

The values for the Mg II index used in this work have been derived from measurements obtained with a series of instruments placed onboard satellites from the National Oceanic and Atmospheric Administration (NOAA) and the National Aeronautics and Space Administration (NASA). As mentioned before, with the help of the overlap between successive missions, a homogenous Mg II index has been generated. The Mg II time series displayed in Figure 3 is based on the work of Viereck et al. (2004), updated to the present [*M. Snow, private communication*]. It is primarily derived using data from the Nimbus-7 SBUV, NOAA-9 SBUV/2 and NOAA-16 SBUV/2 spectrometers, the SUSIM instrument on board UARS, and the SOLSTICE instrument on board SORCE. Viereck et al. (2004) describes the process of merging the individual data sets in more detail. The first observations by Nimbus-7 SBUV took place in November 1978. Starting from that date, the index is generally available 90% of the time. However, some larger gaps exist due to instrumental or orbit control errors, and in these cases, they are filled using data sets from other instruments.

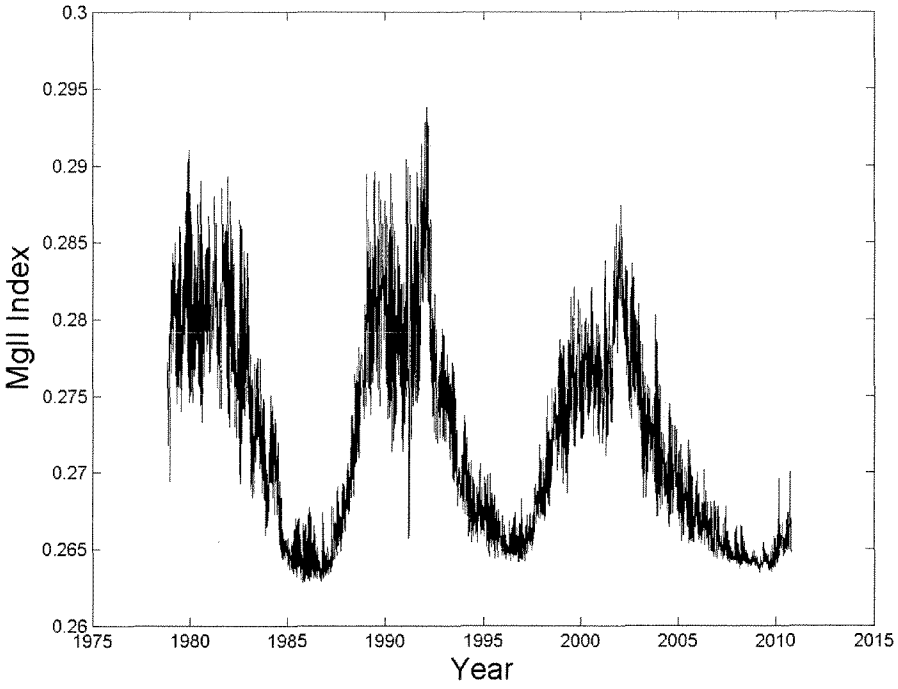
MgII Index
Year
0.3
0.295
0.29
0.285
0.28
0.275
0.27
0.265
0.26
1975
1980
1985
1990
1995
2000
2005
2010
2015

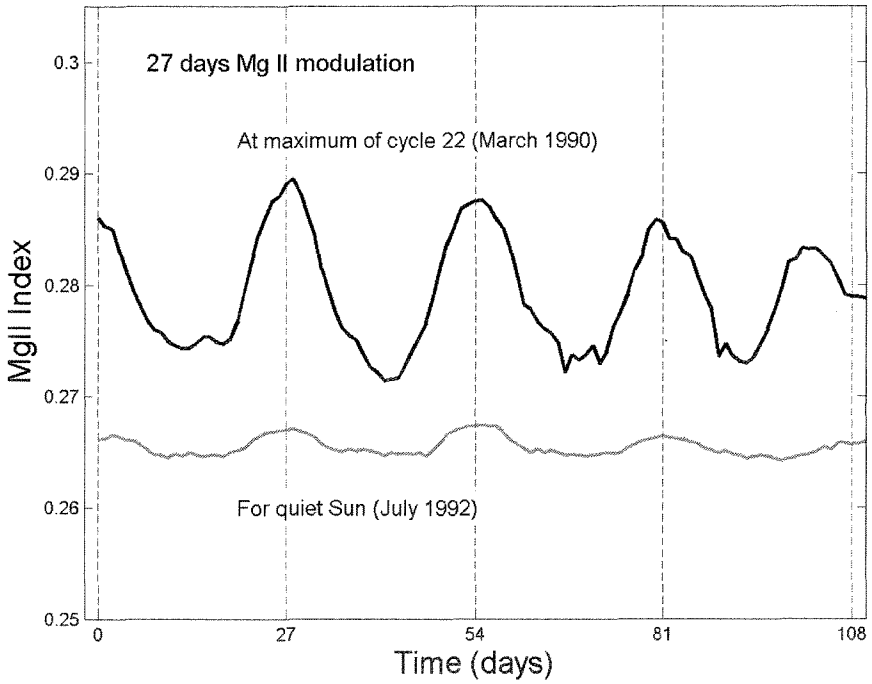
27 days Mg II modulation
At maximum of cycle 22 (March 1990)
For quiet Sun (July 1992)
MgII Index
Time (days)
0.3
0.29
0.28
0.27
0.26
0.25
0
27
54
81
108

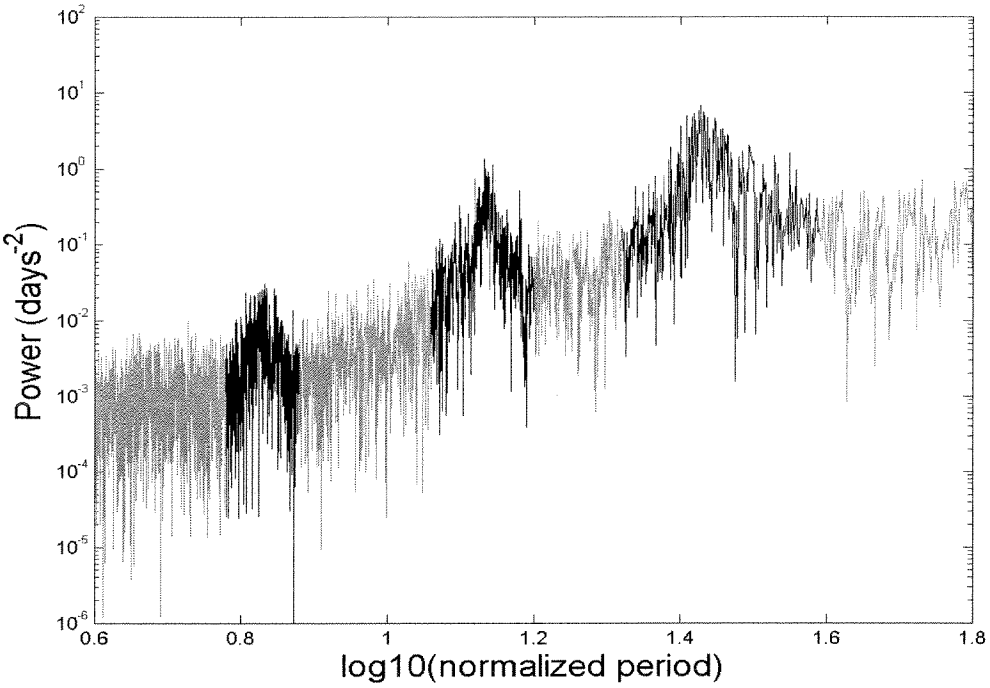

Figure 3: *a*, (upper panel) The Mg II index series from 1978 to 2010 corrected for instrumental effects. *b*, (middle panel) the amplitude of the 27-day rotation effect for two distinct levels of solar activity. *c*, (lower panel) periodogram.

These data clearly show the 11-year cycle, but also contain other periodicities, which may be useful for solar and climate modelling. In particular, Figure 3b shows the 27-day solar rotation effect, whose amplitude typically varies in conjunction with the 11-year solar cycle amplitude (sunspot effect), and Figure 3c is a periodogram showing the 27-day rotation effect and its harmonics of levels 2 and 4. The second harmonic at 13-14 days does correspond to real short-term variations with this period, even though they only occur at selected times during the solar cycle. The presence of such periodicities are important for climate and atmospheric modelling.

2.2 The solar spectrum variability and the Mg II index

2.2.1 Principle

The relationship between the Mg II index and the spectral variability has been studied and modeled by DeLand and Cebula (1993) in the domain 170-400 nm, and Woods et al. (2000) in the domain 120-200 nm. These relationships are described in the next section, and they allow reconstruction of the solar spectral irradiance at different solar activity levels from a chosen spectrum.

The ATLAS 1 and 3 spectra (Thuillier et al., 2004) are composite spectra using SUSIM and SOLSTICE/UARS data from Ly α to 200 nm, SUSIM, SOLSTICE/UARS and SSBUV, SUSIM and SOLSPEC/ATLAS from 200 to 400 nm, SOLSPEC/ATLAS from 400 to 850

nm, and SOSP/EURECA from 800 to 2400 nm. They are used as reference spectra in the reconstruction developed here for the respective dates 29th March 1992, and 11th November 1994, for which the Mg II indices are 0.28300 and 0.26747 respectively. The ATLAS spectra are related to the radiometric scale of the blackbody radiator of the Observatory of Heidelberg, NIST standards of spectral irradiance as determined with tungsten and deuterium lamps, and SURF. The radiometric as well as the wavelength scales are unchanged for the spectra generated from the reference spectrum and a given Mg II index.

These two spectra are chosen as references because of their quasi independence with the measured spectra which were used to establish the Mg II time series, and because of their radiometric agreement with semi-empirical solar spectral models (model C of Fontenla et al. (2005), and Shapiro et al. (2010)).

2.2.2 Methodology

The proxy model to reconstruct the spectral range above 170 nm is based on comparisons between Mg II index and irradiance changes as measured by the SBUV instruments onboard Nimbus 7 and NOAA satellites (DeLand and Cebula, 1993). Below 170 nm, a second proxy model, developed from the SOLSTICE data onboard UARS, is used (Woods et al., 2000). The solar variability can thus be estimated down to the Ly α line. The spectra binned to 1 nm are calculated as follows:

2.2.2.1 The 120–170 nm domain

The proxy model is based on three components representing a constant contribution (for the quiet Sun) and the sensitivity to short-term (solar rotation) and long-term variations (solar cycle). Three wavelengths dependent contrast factors (C, C_S, C_L) and the Mg II proxy are linked to the irradiance (in photon s^{-1} cm^{-2} nm^{-1}) as follows:

$$F^{Mg}(\lambda) = C(\lambda) + C_S(\lambda).MgII^{<3>} + C_L(\lambda).(MgII^{Sol} - MgII^{<3>}) \qquad (1)$$

where $MgII^{Sol}$ is the native Mg II index values from SOLSTICE-UARS that we have scaled on our *MgII* index database as

$$MgII^{Sol} = \alpha(MgII - \beta)$$

with α = 2.6406 and β = 0.1914. $MgII^{<3>}$ is the 81-day (three solar rotations) averaged index for SOLSTICE. For two dates associated to a reference and new Mg II indices, the respective solar fluxes are calculated. Then, the reference spectrum is normalized for the new date using:

$$E^{FUV}_{New}(\lambda) = E^{FUV}_{\mathrm{Re}f}(\lambda).(F^{Mg}_{New}(\lambda) / F^{Mg}_{\mathrm{Re}f}(\lambda))$$

where $E^{FUV}_{\mathrm{Re}f}(\lambda)$ represents the reference spectrum, which is the ATLAS spectrum in our case, and $E^{FUV}_{New}(\lambda)$ represents the new spectrum at the chosen date obtained by using the contrast factors, $F^{Mg}_{\mathrm{Re}f}(\lambda)$ at the date of the reference spectrum and $F^{Mg}_{New}(\lambda)$ at the new date. The result depends on the date because of the 81-day averaged index.

2.2.2.2 The 170–400 nm domain

For this spectral range, a two-component model using scaling factors is used. This factor represents the percent change of solar irradiance for a 1% change in the Mg II index. The daily MgII values (with solar rotational variations) are used. The normalization of the reference spectrum is calculated as follows:

$$E_{New}^{MUV}(\lambda) = E_{Ref}^{MUV}(\lambda).\left[1 + S(\lambda).\left(\frac{MgII_{New}}{MgII_{Ref}} - 1\right)\right] \quad (2)$$

where $S(\lambda)$ is the scaling factor, $E_{Ref}^{MUV}(\lambda)$ is the reference spectrum, $E_{New}^{MUV}(\lambda)$ is the new spectrum. Mg II_{new} and $MgII_{ref}$ are the MgII index at the new date and at the date of the reference spectrum, respectively.

These proxy models provide the solar spectral irradiance recalculated for a given date from a chosen spectrum. We note that for wavelengths longer than 290 nm, the uncertainty in the scaling factor is comparable to the scaling factor itself, which limits the reliability of the reconstructed spectrum.

2.3 The COSI reference spectrum

The choice of the reference spectrum is a crucial point of our technique, since all its possible flaws will be automatically transferred to the entire reconstruction. One possibility is to adopt a theoretical spectrum which is free of measurement noise. Here we investigate this issue by using the theoretical spectrum of the present quiet Sun calculated with COSI by Shapiro et al. (2010) (hereafter referred as the COSI spectrum). Another advantage of this spectrum is its spectral resolution (0.5 pm) which is finer than any available measurement. The COSI performance in reproducing measured spectra was investigated in Shapiro et al. (2010) and Thuillier et al. (2011). It is shown that the COSI spectrum is in very good agreement with the ATLAS 3 spectrum longward of 160 nm, while shortward of 160 nm COSI misses several strong emission lines. Despite these limitations, the continuum level in COSI spectrum is shown to be consistent with the ATLAS 3 spectrum over the entire wavelength domain.

The formation of the solar spectrum in the 160-320 nm range is dominated by a large number of unresolved spectral lines (Haberreiter et al., 2008). Most of these lines have never been measured in the laboratory (Kurucz, 2005), and could be missing in the existing atomic and molecular line lists. As a result, any radiative transfer code has a tendency to underestimate the opacities, and accordingly overestimate the irradiance in this spectral region (Busá et al., 2001; Short and Hauschildt, 2009). To account for these missing lines, Shapiro et al. (2010) introduced additional continuum opacity in 160-320 nm spectral region. This opacity was normalized using SOLSTICE/SORCE measurements for April 2008. As a consequence, the COSI spectrum in the 160-320 nm region is in very good agreement with these measurements. At the same time, Harder et al. (2010) show that the irradiance measured by SOLSTICE/SORCE is approximately 5% smaller than that given by ATLAS 3 in 220-310 nm region. Consequently the COSI spectrum is also 5% below the ATLAS 3 irradiance. To allow for a consistent comparison, we renormalized the COSI opacities in the 160-320 nm range, and removed the 5% systematic difference between ATLAS 3 and COSI spectra in this region. Therefore, using COSI as a reference, the reconstructed spectrum from relation (2) will contain all COSI basic properties.

2.4 The SSI variability

The reconstruction proposed here aims to cover a large range of solar activity. We first use our method to estimate the SSI variability between the minimum and maximum levels of

solar activity. For this purpose, we adopt the mean ATLAS 1 and 3 spectra (date and corresponding Mg II indices are given in section 2.2.1) as reference, which gives us a mean solar activity level. We select the largest and smallest Mg II index as the parameters for Equation (2) with the respective coefficients $S(\lambda)$. This gives us two spectra: one for the largest Mg II index and another for the smallest one. The corresponding ratio of each one of the two reconstructed spectra to the reference spectrum is displayed in Figure 4. We note that between the two extreme maximum and minimum states, the variability at Ly α reaches a factor 2.2. We also see the effect of the solar variability at 280 nm as expected. The upper curve is not symmetrical with the lower one, because the mean spectrum used as reference does not correspond to the mean activity over the period 1978-2010. Note that the same analysis could be performed using COSI, as discussed later on in this paper.

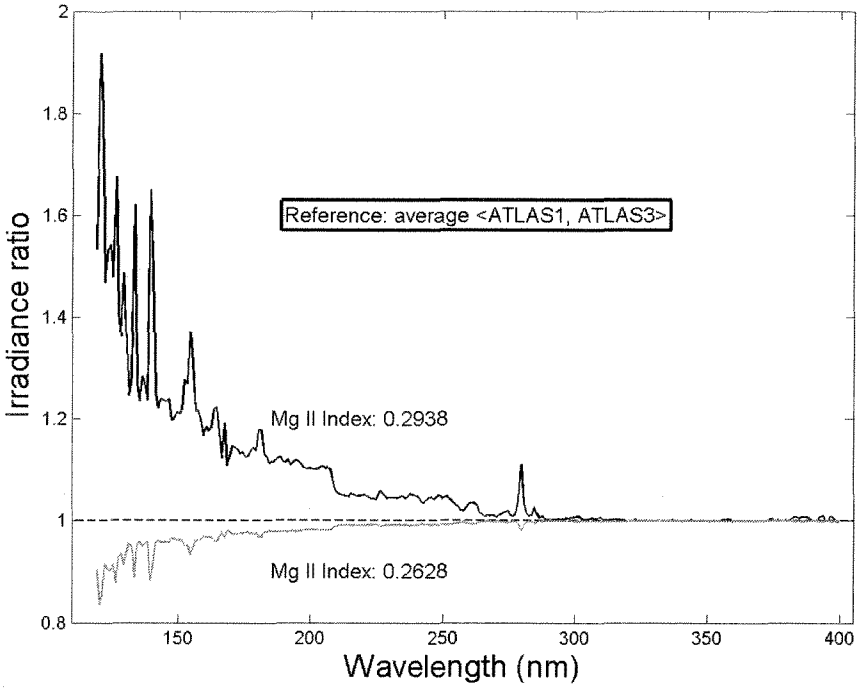

Figure 4: Ratio between the calculated spectra for the minimum and maximum Mg II index with respect to the mean ATLAS 1 and 3 spectra used as reference.

In the literature an available SSI reconstruction is the one provided by Lean (2000). Table 1 compares our results with Lean (2000) and with the SIM and SOLSTICE on board SORCE measurements (Harder et al., 2009 and 2010) between April 2004 and November 2007.

Spectral domain(nm) / author	200-310	310-500
Lean (2000)	0.02	0.04
This work	0.05	0.024*
SORCE	0.16	0.11

Table 1: For the time range April 2004 – November 2007, the irradiance (W/m^2) changes predicted by Lean's model, the present model using Mg II, and the solar spectral irradiance measured by SIM and SOLSTICE (Harder et al., 2009 and 2010) on board SORCE, are shown. The data from line 2 is extracted from Table 1 of Haigh et al. (2010). The asterisk indicates that the calculation has been carried out only up to 410 nm.

We see that the reconstruction based on the Mg II index provide a value for irradiance between Lean (2000) and SORCE for both spectral intervals. For the spectral range between 310 and 500 nm, although our calculation extends only up to 400 nm this restriction in wavelength cannot explain the differences in values observed here. It is possible that the difference is due to the Lean (2000)'s model variability, which uses sunspot darkening to represent solar activity effect at wavelength greater than 300 nm. The largest differences are observed between SORCE and the two other reconstructions.

One factor to consider is that aging of instruments in space typically decreases their responsivity. While corrections can be made by different approaches, their precision remains difficult to estimate. Although it is possible that aging could contribute to partly explain the spectral irradiance variability shown by SIM-SORCE, this contribution is difficult to estimate. Ball et al. (2011) and Lockwood (2011) discuss this issue in more detail.

As an interesting exercise we use our method to study the solar irradiance levels during the solar minimum activity in the transition between cycle 23 and 24. Indeed, the ATLAS 3 spectrum (November 1994), used here as the reference, was measured at low solar activity (F10.7 = 77 units and sunspot number = 16). However, it was an activity level greater than observed around June-July 2008 (Woods et al, 2009) which was in fact the smallest since irradiance measurements from space are available. The ratio of the calculated spectrum for July 2008 to ATLAS 3 is displayed in Figure 5, which shows for example that the Ly α line intensity was about 10 % lower than in November 1994.

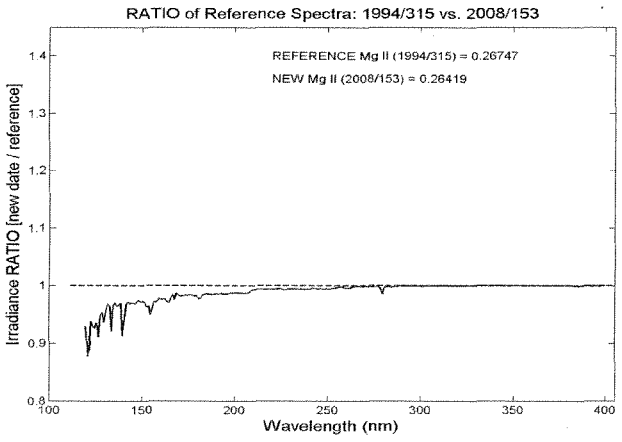

Figure 5: Ratio of the calculated spectrum at the minimum of solar activity between cycle 23 and 24 to ATLAS 3 using the Mg II modelling.

Now, we investigate the performance of our method by comparing reconstructions with recent measurements by SIM on board SORCE and by SOLAR on board the Space Station

(ISS). SOLAR-ISS spectrum (Thuillier et al., 2011) is made of three data sets: SOLSPEC above 170 nm, SOL-ACES below 134 nm (Schmidtke et al., 2006) and SOLSTICE-SORCE to fill the gap. The reference spectrum being ATLAS 3, we calculate the predicted spectrum for June 1, 2008. The ratios of the measured spectrum by SOLAR-ISS and SIM-SORCE to the respective reconstructions are displayed in Figure 6. This figure shows high frequency oscillations, which are due to the wavelength scale difference between the measurement and its reconstruction (a similar phenomenon will be seen in Figure 8). In average, the ratio is about 5 % lower than unity, indicating that the reconstructed irradiance is greater than the measurements obtained from both instruments. An important aspect is that this ratio is strongly wavelength dependent as it is close to unity between 180 and 220 nm, approaching unity above 290 nm while the largest difference is found around 250 nm.

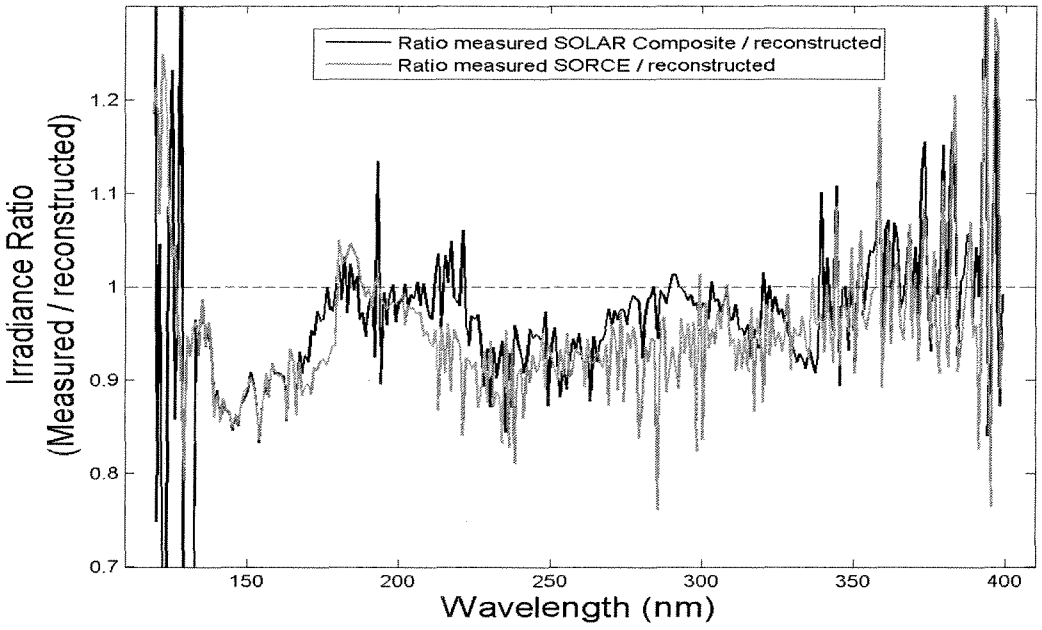

Figure 6: Ratio of the measured spectra by SOLSPEC-ISS and SIM-SORCE to the reconstructed spectrum at the minimum of solar activity between cycle 23 and 24.

Over a given spectral domain (e. g. 150-200 nm), we calculate the mean difference of the ratio with respect to unity of the reconstructed to the measured spectra. It will be labelled as Δ and shown as a function of the spectral domains in Table 2.

Spectral domain (nm)	120-150	150-200	200-250	250-300	300-350	350-400
Δ1 (SOLAR-ISS)	11.3	5.3	4.1	4.0	3.3	2.9
Δ2 (SORCE)	3.7	5.7	8.0	7.9	4.9	0.9

Table 2: Mean difference (%) with respect to unity of the ratio between the reconstructed SOLAR-ISS, and SIM and SOLSTICE on board SORCE spectra from ATLAS 3 and the corresponding measurements.

This demonstrates the agreement between the ratios in the range 150-200 nm. Above 200 nm, Mg II reconstruction is closer to the SOLAR-ISS spectrum than SIM-SORCE irradiance. However, below 150 nm, the situation reverses. It can be explained by the fact that this part of the spectrum in fact originates from the SOL-ACES spectrometer, which observes EUV irradiances slightly smaller than those measured by the SORCE instruments (Schmidtke, 2008). It is important to mention that the two measured spectra are consistent within their own accuracy.

2.5 Accuracy of the reconstructions.

Direct comparison of reconstructed irradiance spectra with time series of satellite data is dependent on the accuracy of the long-term instrument degradation corrections, which have a complex spectral and temporal dependence. Examples of such comparisons are shown by DeLand and Cebula (2008) and references therein. To estimate the accuracy of a single reconstructed spectrum, we use the ATLAS 1 and ATLAS 3 spectra, which are independent from the Mg II index time series described in Section 2.1.

Starting from the ATLAS 3 data obtained at low solar activity, we calculate the ATLAS 1 spectrum using the Mg II index at this time. To show the accuracy of the reconstructed spectrum, we calculate the ratio of the latter to the measured spectrum. The ratio is displayed in Figure 7 (solid line). The ratio decreases from 4% to less than 1% as the wavelength increases from 170 to 400 nm.

Similarly, we reconstruct the ATLAS 1 spectrum using the COSI reference spectrum, and we calculate its ratio to the measured ATLAS 1 spectrum, also shown in Figure 7 (dash line). Up to 330 nm, the differences between the two reconstructions are lower than 1%. Around 340 nm, COSI shows an oscillation reaching 7% due to some strong molecular bands of CN, NH, and OH. The origin of the feature around 340 nm may be associated to the lack of knowledge on the position and oscillator strengths of the lines in these bands.

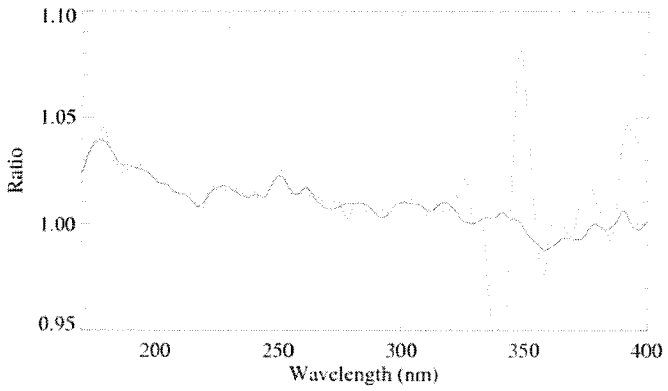

Figure 7: Ratios of the reconstructions of ATLAS 1 using the Mg II modelling and the COSI reference spectrum, solid line and dashed line,

respectively. The solid line refers to the reconstructed spectrum using ATLAS 3 as a reference, and the dotted line is produced using the COSI-spectrum as a reference. To remove the noise and allow for a better comparison, the ratios are smoothed with a Gaussian shape of 5 nm width at half maximum.

This figure also shows that the agreement between the two reconstructions is remarkably good as differences are about half a percent; however, they are wavelength dependent. Table 3 lists the mean difference (with respect to unity) of the ratio of the reconstructed spectrum to the measured spectrum at different spectral regions. In the range 170-200 nm, the reconstruction based on COSI-spectrum is slightly better than the one based on ATLAS 3 spectrum by 0.7 percent. Above 200 nm, the accuracy provided by each model is comparable and remains wavelength dependent. We note that below 150 nm, the accuracy of the Mg II reconstruction decreases reaching 3.7% at Ly α. However, this ratio is consistent with the uncertainty of the ATLAS 3 spectrum.

Δλ (nm)	120-150	150-200	200-250	250-300	300-350	350-400
Δ1	3.7	3.6	1.3	1.0	0.5	0.7
Δ2	N/A	2.9	1.7	0.9	0.2	1.0

Table 3: Mean difference Δ1 in percentage, with respect to unity, of the ratio between the reconstructed ATLAS 1 from ATLAS 3 using the Mg II index and the measured ATLAS 1, and mean difference Δ2, with respect to unity, of the ratio between the reconstructed ATLAS 1 by COSI and the measured ATLAS 1 as a function of the wavelength domain.

Another estimate of the accuracy of the reconstruction is performed using a spectrum (29 March 1992) from the UARS mission (Rottman et al., 2001). Adopting ATLAS 3 and the COSI-spectrum as references, we reconstruct the SOLSTICE/UARS spectrum and compare them with the original one, as shown in Figure 8.

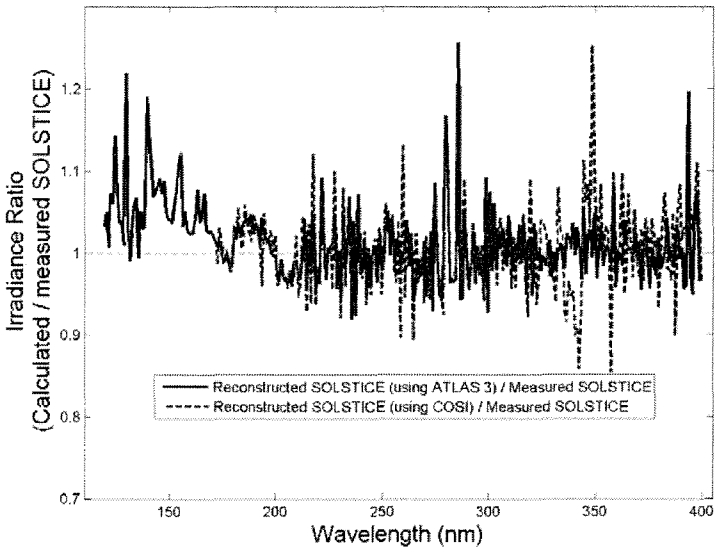

Figure 8: Ratio of the reconstructed SOLSTICE spectrum using ATLAS 3 as reference for March 29, 1992 to the measured SOLSTICE spectrum on board UARS on the same day, and ratio of the reconstructed SOLSTICE spectrum using COSI to the measured SOLSTICE spectrum on the same day.

Using ATLAS 3 or COSI as reference spectrum does not change significantly the reconstructed spectra, which appear very close to the measurement, especially above 200 nm. Below 200 nm, the two reconstructed spectra remain very close to each other, but their ratio to the measurement shows a difference reaching 8 % below 150 nm. As already seen on Figure 6, the oscillations of the two ratios are generated by a slight wavelength difference between the reconstructions and the original data. The RMS difference between the reconstructed SOLSTICE and the measured SOLTICE spectrum in several spectral domains is listed in Table 4. As already noted, the Mg II reconstruction does not work with the same precision above 150 nm compared to below 150 nm.

$\Delta\lambda$ (nm)	120-150	150-200	200-250	250-300	300-350	350-400
$\Delta 1$	6.5	3.0	0.8	0.1	0.6	0.3
$\Delta 2$	NA	1.8	0.8	0.9	0.03	0.6

Table 4: Mean difference $\Delta 1$ (in percentage) with respect to unity of the ratio between the reconstructed SOLSTICE from ATLAS 3 using the Mg II modelling and the measured SOLSTICE, and mean difference $\Delta 2$ with respect to unity of the ratio between the reconstructed SOLSTICE by COSI and the measured SOLSTICE spectrum as a function of the wavelength domain. The SOLSTICE spectrum was measured on 29 March 1992.

3. Reconstruction of the solar spectral irradiance prior to 1978

3.1 The relation between the modulation potential and Mg II index

Prior to 1978, very few measurements of the solar spectrum exist and what is available has low accuracy which makes its use questionable. Consequently, the use of proxies is unavoidable. Available data for the Mg II index span over a few decades. Extension in time would then require using another index. The obvious choice would be sunspot number time series. However, their quality decreases towards the past, and periods such as the Maunder Minimum, which are interesting from the climate perspective, are obviously poor in solar information. Alternatively, a widely used proxy for long term solar activity is the solar modulation potential, which is the measure of the heliospheric shielding from cosmic rays (Lockwood et al., 1999). The neutron monitor data, available since 1950s, allow to reconstruct the modulation potential for the last few solar cycles with monthly resolution (Usoskin et al., 2005), while the cosmogenic isotope data allows to reconstruct the modulation potential with decadal resolution back to 7000 BC (McCracken et al., 2004). We analyse then the correlation between the neutron monitor and Mg II index data. In Figure 9 we show that the yearly mean values of the modulation potential Φ from Usoskin et al. (2005) are in good correlation with yearly mean values of the Mg II index.

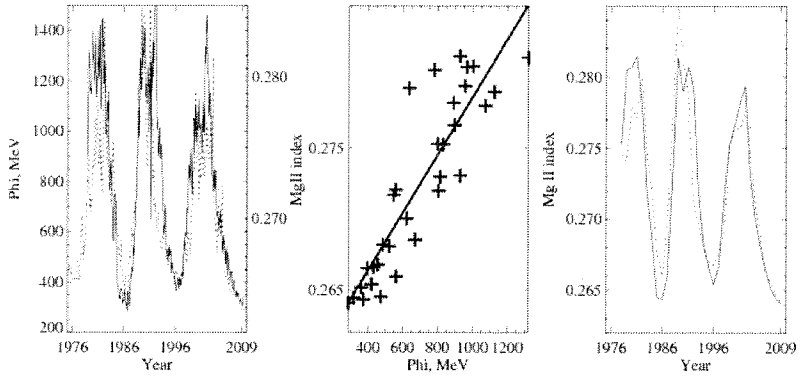

Figure 9: *a*, (left panel) shows the variation with time of the Mg II index (solid line) and the modulation potential (dotted line) data between 1978 and 2010. *b*, (central panel) shows the relationship between the yearly mean of the Mg II indices and neutron monitor data sets. The heavy straight line results from a linear fit between these two datasets. *c*, (right panel) shows the variations of the yearly mean values of the measured (solid line) and reconstructed from modulation potential (dotted line) Mg II index.

The straight line shown in Figure 9b is represented by:

$$\text{Mg II} = a + b\,\Phi \qquad (3)$$

The coefficients a and b, as well as the Pearson correlation coefficients are given in Table 5. The maximum correlation is obtained when the time lag between the modulation potential and the Mg II index equals to 7 months. For the whole data, the results of the linear fit are given in Table 5, left column (all results).

Coefficients/data	All data	Subset 1 (1982-1990)	Subset 2 (1991, 1993-2009)
a	0.25823 ± 0.0015	0.25564±0.0009	0.2572±0.0008
b	2.032e-05±1.92e-6	1.990e-05±1.036e-6	2.243e-05±1.26e-6
Correlation	0.887	0.991	0.975

Table 5: Coefficients of the linear regression as well as correlations obtained with the full dataset and the two subsets shown in Figure 10. The error bars correspond to the 1 σ statistical uncertainty.

The accuracy of the Eq. (3) linear fitting is illustrated in Figure 10. One can see that the uncertainty distribution is not Gaussian and after the removal of several outliers (prior to 1982 and 1992 Mg II measurements) has a bimodal structure as well as being time dependent. The errors within each of the two selected subsets (marked in Figure 10) have reasonably random distribution. The Pearson correlation calculated individually for each of the subsets is significantly higher than calculated for the entire dataset (see Table 5, last line). Such behaviour could be caused by some inhomogeneities in the Mg II dataset prior to 1991. However, Viereck et al. (2004) discussed the use of multiple Mg II data sets to create a final composite product, with transitions between individual data sets in March 1991, October 1992, and August 2001. The choice of each data set and the period when it was used were evaluated to minimize any residual trend or biases in the final composite Mg II product.

Thus, it cannot be excluded that the bimodal distribution shown on Figure 10 can be indication of three possible effects: a change in solar behaviour as represented by the modulation potential relative to the Mg II index, an instrumental effect, or the method used for the Earth magnetic field strength correction.

The regression coefficients a and b calculated separately for the two discussed subsets are given in Table 5, while linear fits for these two subsets are presented in the middle and lower panels of Figure 10. It is noticeable that the linear fits are better in case of the two subsets (Figure 10 middle and lower panels) than in Figure 9b for the whole set.

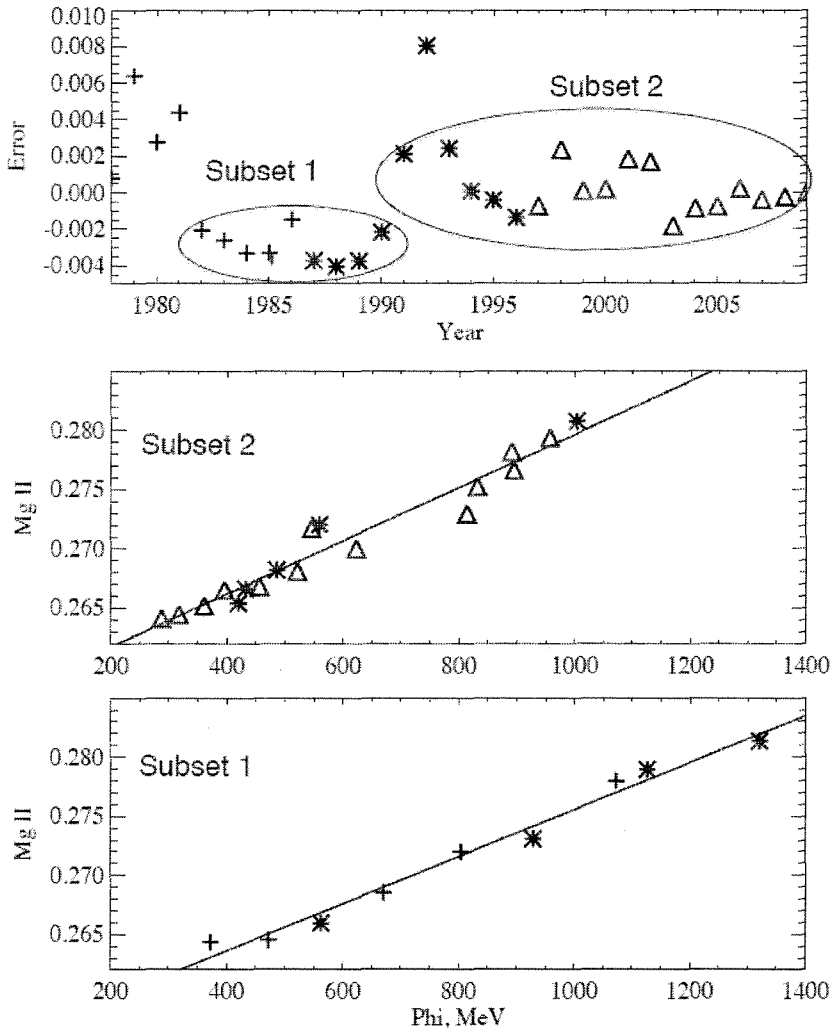

Figure 10: The upper panel shows the uncertainties affecting the linear regression between the modulation potential data and the Mg II index as a function of time. The middle and lower panels show the relationship between the Mg II index and modulation potential for the two data subsets. Data for cycles 21, 22, and cycle 23 and beginning of cycle 24 are shown by signs +, stars and triangles, respectively.

We will use the two linear fits (subset 1 and 2) in section 3.4 to estimate of the uncertainty generated by the data used with the present method for the reconstruction of the past solar spectral irradiance.

3.2 The reconstruction of the past SSI

Figures 9 and 10 are a relative calibration of the neutron monitor and Mg II proxies in their period of overlap. As in general, we do not have the solar magnetic field for the past periods, we assume that this calibration is still valid in the past. Different solar activity regimes may alter the neutron flux/Mg II index relationship, however to an unknown extent.

Using the correlation between the modulation potential and Mg II index allows us to reconstruct the Mg II index from the modulation potential and derive the past SSI. Our assumptions are:

i) the linear relationship between the Mg II index and the modulation potential does not change with time and therefore is applicable for historical reconstructions,
ii) the technique presented in Section 2.2.1 can be used, i.e. Eqs. (1-2) can be applied for periods other than the range 1978-2010.

The historical data of the modulation potential are obtained from the records of the cosmogenic isotopes concentration (which are spallation products of galactic cosmic rays). We base our reconstruction on the South Pole and DYE 3 ^{10}Be data from McCracken et al. (2004), which give the modulation potential with a 22-year resolution. To homogenize these datasets, we normalized them to the local interstellar spectra from Castagnoli and Lal (1980) as explained in Shapiro et al. (2011a). As the historical records of the modulation potential are available with a 22-year resolution, our long-term reconstruction has the same resolution. We applied the Eqs. (1-2) to the 22-year averaged data (note that the last term of Eq. (1) will disappear). For this, we first average the Eqs. (1-2) over the period 1978-2010 and calculate the mean solar spectrum for the period 1978-2010. Then we use this spectrum as a reference and the mean value of the Mg II index as a corresponding reference value of the solar activity. Finally, using the Mg II index reconstructed from the modulation potential, we can calculate the solar irradiance as far back in the past as the ^{10}Be data are available.

McCracken et al. (2004) gives two datasets of the modulation potential: one measured at DYE 3, Greenland, another at South Pole. According to the South Pole data, the minimum value of the 22-year averaged modulation potential for the last 400 years equals to 162 MeV, and was reached in 1706. This value corresponds to the mean value of modulation potential for the 1696-1717 period. According to the DYE 3 data the minimum value of the modulation potential equals to 128 MeV and was reached in 1704. These two values represent the minimum state of activity of the Sun during the Maunder Minimum, and they disagree by 20 %. Furthermore, as the accuracy of these measurements is not given, we shall use these two values to estimate the accuracy of the reconstruction. For that, in Table 6 we give the corresponding values of the Mg II index, calculated with the different sets of the regression coefficients as explained in Section 3.1.

Derived Mg II index	Subset 1	Subset 2
South Pole data	0.2589±0.0011	0.2608±0.0010
DYE3 data	0.2582±0.0010	0.2600±0.0010

Table 6. Minimum values of the derived Mg II index for the last 400 years, calculated with different cosmogenic isotope datasets and regression coefficients.

From Table 6 the derived Mg II index during the Maunder Minimum is constrained between 0.2572 and 0.2618 (see discussion in Sect. 3.3) with the mean value equal to 0.2595. These values are used to calculate the corresponding spectrum. We note that while the Maunder Minimum lasted almost an entire century (1645-1710) based on sunspot records, we will refer to the Maunder Minimum spectrum as calculated for the minimum state of the Sun activity inferred from the cosmogenic isotope data. According to these data the solar

minimum activity was reached in the beginning of 18th century (see previous paragraph), while a moderate sunspot activity was already observed.

In Figure 11 we give the ratio for the reconstructed Maunder Minimum irradiance using ATLAS 3 as reference to the measured ATLAS 1 (left panel) and ATLAS 3 (right panel) spectra. The solid line corresponds to the Maunder Minimum irradiance calculated assuming the mean value (0.2595) of the derived Mg II index (mean of the four values given in Table 6), and the linear relationship shown in Figure 9. The accuracy of this reconstruction will be discussed in section 3.4.

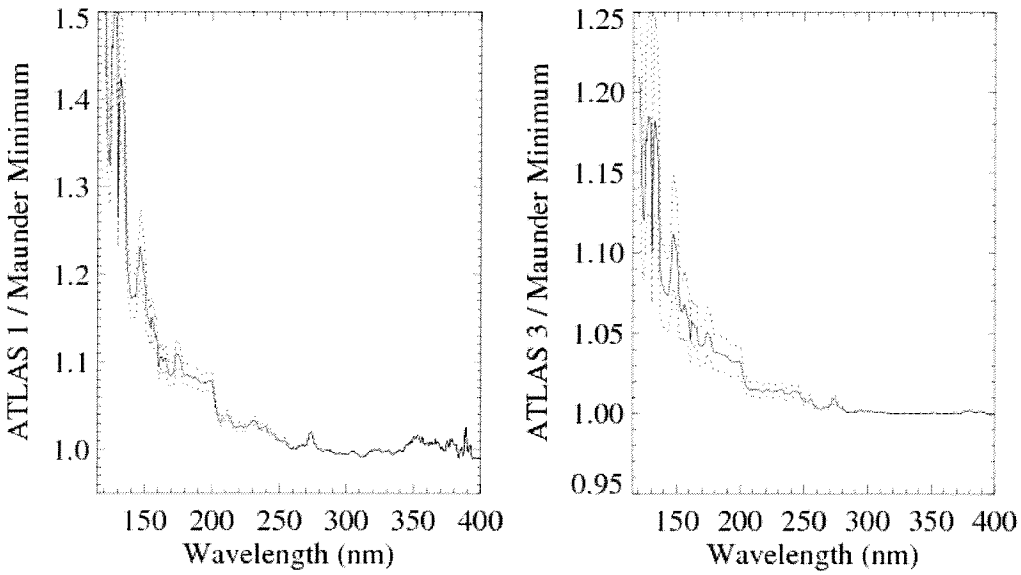

Figure 11: Ratios of the ATLAS 1 (left panel) and 3 (right panel) spectra to the Maunder Minimum spectrum. The dotted lines indicate the uncertainty of our approach.

Figure 11 shows that the differences in SSI are wavelength dependent and the 1706 SSI was smaller than the values measured during the minimum of the solar cycle 21 by ATLAS 3. In particular, our analyses suggests that for the 1706 SSI reconstruction, the Ly α irradiance was 20% lower than for ATLAS 3 period, which was close to the minimum of the cycle 22. Note that for wavelength larger than 300 nm there is no predicted SSI variability between the Maunder Minimum and the present time.

Now, we estimate the SSI change in the Ly α - 400 nm spectral interval by several authors and compare with our results. Integration of the SSI over this range gives 110.11 W/m^2 for the Maunder Minimum.

Authors	ΔSSI (Ly α - 400 nm)
Lean (2000)	0.8 W/m^2
Krivova et al. (2010)	0.5 W/m^2
Shapiro et al. (2011)	4.1 W/m^2
This article	0.2 W /m^2

Table 7: Comparison between different approaches of the SSI variation in the interval Ly α-400 nm between the mean irradiance during the cycle 22 and the irradiance during the Maunder Minimum.

These four results are different, but three are about in the same range. This illustrates that different hypothesis for reconstructions generate different results.

3.4 Accuracy of our SSI reconstruction

Solar activity is described by different proxies, among them we have chosen those having an overlapping period and different coverage in time. Figures 9 and 10 are a relative calibration of the neutron monitor and Mg II proxies in their period of overlap. As in general, we do not have the solar magnetic field for the past periods, we assume that this calibration is still valid in the past.

The uncertainty of our reconstruction originates from several inputs:

i) The reference spectrum,
ii) The method of reconstruction from a set of coefficients, also a few percents as shown in Section 2.5;
iii) The accuracy of the regression coefficients in the Eq. (3);
iv) The uncertainty of the historical values of the modulation potential.

The chosen spectrum accuracy is generally known. Its accuracy (i) is wavelength dependent. For the ATLAS 3 spectrum used in this article, the accuracy is 2 to 3% (Thuillier al., 2004) above 200 nm. Accuracy (ii) has been addressed by DeLand and Cebula (2008) who have generated a composite SSI from 1978 to 2005 by merging different satellite data sets. These spectra were compared with published synthetic irradiance data from Lean et al. (2005), who use the Mg II index as a proxy for facular variations. These two data sets generally agree within ±2% over most spectral and temporal ranges, with some exceptions below 140 nm and after 2002.

The final uncertainty results from the combination of the above sources of uncertainties. The uncertainties (i) and (ii) are mainly systematic and will not strongly affect the change of the irradiance. Uncertainty (iii) is discussed in Section 3.1. Uncertainty (iv) originates from the historical values of the modulation potential, which is not known. This is why we have used the two different values found at South Pole and DYE 3 data as an estimate of the cosmogenic isotopes concentration.

To take into account the possible uncertainties affecting the South Pole and DYE 3 and the Mg II data, we have considered the smallest and greatest constraints of the derived Mg II index from Table 6 obtained by using the lowest value 0.2572 and the highest value 0.2618 at one σ. The corresponding spectra are compared to ATLAS 1 and ATLAS 3 and displayed as dotted lines in Figure 11.

Consequently the changes of the Mg II index between the Maunder Minimum and ATLAS 1 and ATLAS 3 periods are 0.0235±0.0023 and 0.0079±0.0023, respectively. According to our approach the change of the SSI linearly depends on the change of the Mg II index. Therefore the reported uncertainty of the Mg II index change directly transfers to the uncertainty of the spectral irradiance change. Thus the uncertainty of the forcing between the ATLAS 1 period and the Maunder Minimum can be estimated as 10% (0.0023/0.0235), while the uncertainty of the forcing between the ATLAS 3 period and the Maunder Minimum is 30% (0.0023/0.0079). These uncertainties are indicated on Figure 11.

Our method is based on the extrapolation of the Mg II and modulation potential relationship, and we assumed that Eqs. (1-2), established from the observations during the several solar cycles, could also be used to calculate the solar variability during the last 400 years. This is equivalent to the assumption that the same mechanism is in charge of the 11-year cycle and of the long-term trend. The basic reason of this assumption is that the UV SSI depends on the solar magnetic field. A similar assumption was employed by Steinhilber et al. (2009) who extrapolated the relationship between the TSI and the open magnetic flux. They obtained 0.9±0.4 W/m^2 change between the present time and Maunder Minimum solar-cycle averaged TSI values.

Shapiro et al. (2011a) made another assumption and stated that 11-year cycle and the long-term trend have a different origin. They assumed that the minimum state of the quiet Sun in time corresponds to the observed quietest area on the present Sun. Then, they used the 22-year smoothed modulation potential values which were assumed to be a proxy of the long-term solar activity, to interpolate between the present quiet Sun and the minimum state of the quiet Sun. Using the same dataset of the modulation potential as employed in the present paper, they obtained 6.4±3.2 W/m^2 TSI change between the present time and the Maunder Minimum. On the other hand Schrijver et al. (2011) argued that the Sun was in the minimum state of its activity during the 2008-2009 minimum. This leaded them to the conclusion that the Sun was in the same condition during the Maunder Minimum as in 2008-2009. Such a conclusion is close to the small SSI variability provided by our method (Table 5, last line).

It is important to note that each recently published long-term reconstruction is based on the set of assumptions which cannot be unambiguously proved or disproved with presently available observational data.

4. Conclusion

We provide a new method to reconstruct the SSI within the 120-400 nm spectral domain from a reference spectrum using the Mg II index for the present time and the neutron monitor data for the past. The calibration of the neutron monitor data versus the Mg II index is first established for the recent period (1978 to now), then it is applied to the past using the cosmogenic isotopes data. The advantage of this new method is that it can be re-accessed by more accurate laboratory measurements and/or re-processing of solar spectra to derive the Mg II index.

The solar spectrum variability has been analysed using the Mg II index as a proxy. A set of coefficients is derived allowing the reconstruction of a spectrum at a date for which the Mg II is known. We have estimated the accuracy of this method by comparing reconstructions and observations. We have also searched for the lowest solar spectral irradiance and compare the prediction with observations independently made on board UARS, SORCE and SOLAR-ISS.

The correlation between the neutron monitor data with the Mg II index is used to extend the reconstruction beyond the availability of the Mg II data, i.e. before 1978. We have derived the SSI in the range 121-400 nm for the Maunder Minimum (which corresponds to the

beginning of 18th century according to cosmogenic isotope data). Following this approach we obtain that in this range the mean change is 0.2 W/m^2 with respect to the mean irradiance and a change of 20% in amplitude at Ly α with respect to the minimum of solar cycle 22.

Acknowledgements Part of this work has been supported by LATMOS of Centre National de la Recherche Scientifique and Centre National d'Etudes Spatiales (CNES) in preparation of the PICARD mission. M. DeLand was supported by NASA contract NNH06HX18C. S.M.L. Melo acknowledges the support she received from the Canadian Space Agency for the participation in the PICARD mission. W. Schmutz and A. Shapiro acknowledge the support from the European Community's Seventh Framework Programme (FP7/2007-2013) under grant agreement N 218816 (SOTERIA) and from Swiss National Science Foundation under grant CRSI122- 130642 (FUPSOL). D. Bolsee from the Institut d'Aéronomie Spatiale de Belgique (IASB) acknowledges the support from the Belgian Solar-Terrestrial Centre of Excellence (STCE). The SOLSPEC investigation has been developed by LATMOS-CNRS (France), IASB and Landesternwarte (LSW) from Heidelberg (Germany), was supported by CNES, sponsored by ESA and run by B-USOC.

References

Austin, J., et al.:2008, *J. Geophys. Res.*, **113**, D11306, doi:10.1029/2007JD009391.

Avrett, E. H.: 1992, *Proceedings of the Workshop on the Solar Electromagnetic Radiation Study for Solar Cycle 22 (Ed. R.F. Donnelly), National Technical Information Service*, Springfield, VA, 20–42.

Ball, W. T., Unruh, Y. C., Krivova, N. A., Solanki, S., Harder, J. W.: 2011, *Astron. Astrophys.*, **530**, A71, doi:10.1051/0004-6361/201016189.

Bolduc, C., Charbonneau, P., Bourqui, M. S., A.D. Crouch, A. D.: 2011, *Solar Phys.* submitted.

Busá, I., Andretta, V., Gomez, M. T., and Terranegra, L.:2001, *A&A*, **373**, 993.

Castagnoli, G., and Lal, D.: 1980, **22**, 133.

Cebula, R. P., and M. T. DeLand.:1998, *Solar Phys.* **177**, 117.

Cebula, R. P., DeLand, M. T., Schlesinger, B. M.: 1992, *J. Geophys. Res.*, **97**, D11, 11,613-11,620.

Cebula, R., Thuillier, G., VanHoosier, M., Hilsenrath, E., Hersé, M., and Simon, P.: 1996, *Geophys. Res. Lett.* **23**, 2289.

DeLand, M. T., and Cebula, R. P.: 1993, *J. Geophys. Res.*, **98**, 12,809-12,823.

DeLand, M. T. and Cebula, R. P.: 2008, *J. Geophys. Res.*, **113**, A11103, doi:10.1029/2008JA013401.

Egorova, T., Rozanov, E., Hochedez, J.-F., and Schmutz, W.: 2008, *Atmos. Chem. Phys.*, **8**, 2965-2973.

Haberreiter, M., Schmutz, W., and Hubeny, I.: 2008, *A&A*, **492**, 833, 2008.

Harder, J. W., Fontenla., J. M., Pilewskie, P., Richard, E. C., and Woods, T. N.: 2009, *Geophys. Res. Lett.* **36**, LO7801.

Harder, J. W., et al.: 2010, *Solar Phys.* **263**, 3-24, 2010.

Haigh, J.D., Winning, A. R., Tourmi, R., and Harder, J. D.: 2010, *Nature*, **467**, 696.

Heath, D. and Schlesinger, B. M.: 1986, *J. Geophys. Res.*, **91**, 8672.

IPCC, Climate Change 2007: The Physical Science Basis, Contribution of Working Group I to the Fourth Assessment Report of the Intergovernmental Panel on Climate Change, S. Solomon et al., Eds. (Cambridge Univ. Press, Cambridge).

Krivova, N. A., Vieira, L. E. A., and Solanki, S. K.: 2010, *J. Geophys. Res.*, **115**, A12112, doi:10.1029/2010JA015431.

Kurucz, R. L.: 2005, Including all the lines, *Mem. Soc. Astron. Ital. Suppl.*, **8**, 86.

Lean, J. L., White, O. R., Livingston, W. C., Donnelly, R. F., and Skumanich, A.: 1982, *J. Geophys. Res.*, **87**, 10307.

Lean, J.: 2000, *Geophys. Res. Lett.* **27**, 2425.

Lean, J., Rottman, G., Harder, J. and Kopp, G.: 2005, SORCE contributions to new understanding of global change and solar variability, *Solar Phys.*, **230**, 27– 53.

Lockwood, M., Stamper, R. and Wild, M. N.: 1999, *Nature*, **399**, 437.

Lockwood, M.: 2011, *J. Geophys. Res.*, **116**, D16103, doi:10.1029/2010JD014746.

McCracken, K. G., McDonald, F. B., Beer, J., Raisbeck, G., and Yiou, F.: 2004, *J. Geophys. Res.* **109**, 12103.

Neupert, W. M.: 1998, *Solar Phys.*, **177**, 181.

Rottman, G. J., Woods, T. N., Snow, M., and De Toma, G.: 2001, *Adv. Sp. Res.*, **27**, 1927.

Rottman, G. J.: 2005, *Solar Phys.* **230**, 1, 7.

Schmidtke, G., Brunner, R., Eberhard, D., Halford, B., Klocke, U., Knothe, M., Konz, W., Riedel, W.-J., Wolf, H.: 2006, *Adv. Space Res.*, **37**, 273.

Schmidtke, G.: 2008 SOL-ACES EUV irradiance, presented at the Fraunhofer Institute solar meeting, May 2008.

Schrijver, C. J., Livingston, W. C., Woods, T. N. and Mewaldt, R. A.: 2011, *Geo. Res. Lett*, **38**, L06701, doi:10.1029/2011GL046658.

Semeniuk, K., Fomichev, V. I., McConnell, J. C., Fu, C., Melo, S. M. L., and Usoskin, I. G.: 2010, *Atmos. Chem. Phys. Discuss.*, 10, 24853-24917, doi:10.5194/acpd-10-24853.

Shapiro, A., Schmutz, W., Schoell, M., Haberreiter, M., and Rozanov, E.: 2010, *A & A*, **517A**, 48S.

Shapiro, A. I.; Schmutz, W.; Rozanov, E.; Schoell, M.; Haberreiter, M.; Shapiro, A. V.; Nyeki, S.: 2011a, *A&A*, **529**, A67.

Shapiro, A. V., Rozanov, E., Egorova, T.; Shapiro, A. I., Peter, Th.; Schmutz, W.: 2011b, *J. Atmos and Solar-Terr. Phys*. **73**, 2-3, 348.

Short, C. I., and Hauschildt, P. H.: 2009, *ApJ*, **691**, 1634.

Solomon, S., K. H., Rosenlof, R. W., Portmann, J. S., Daniel, S. M., Davis, T. J., Sanford, G-K. Plattner.: 2010, *Science*, [DOI:10.1126/science.1182488], **327**, 1219.

Steinhilber, F., Beer, J., and Fröhlich, C.: 2009, *Geophys. Res. Lett.*, **36**, L19704, doi:10.1029/2009GL040142.

Tapping, K. F.: 1987, *J. Geophys. Res.*, **92D1**, 829.

Thuillier, G., Floyd., L., Woods, T.N., Cebula, R., Hilsenrath, E., Hersé, M., and Labs, D.: 2004, in Solar Variability and its Effect on Climate, *AGU monograph* **141**, eds J. Pap and P. Fox, p. 171.

Thuillier, G.; Claudel, J.; Djafer, D.; Haberreiter, M.; Mein, N.; Melo, S. M. L.; Schmutz, W. Shapiro, A.; Short, C. I.; Sofia, S.: 2011, *Solar Phys*. **268**, 125.

Thuillier G., Bolsée, D., Foujols, T., Schmidtke, G., Nikutowski, B., Brunner, R., Hersé, M., Gillotay, D., Mandel, H., Petermanns, W., and Decuyper, W., 2011, to be submitted to *Solar Phys.*

Usoskin, I. G., Alanko-Huotari, K., Kovaltsov, G. A., and Mursula, K.: 2005, *J. Geophys. Res*. **110**, A12108, doi:10.1029/2005JA011250.

Viereck, R. A., Floyd, L. E., Crane, P. C., Woods, T. N., Knapp, B. G., Rottman, G., Weber, M., Puga, L. C., and DeLand, M. T.: 2004, *Space Weather*, **2**, S10005, doi:10.1029/2004SW000084,

Woods, T. N., Tobiska, W. K., Rottman, G. J., and Worden, J. R.: 2000, *J. Geophys. Res.*, **105**, A12, doi:10.1029/2000JA000051.

Woods, T., N., Chamberlin, Ph. C., Harder, J. W., Hock, R., A., Snow, M., Eparvier, F. G., Fontenla, J., McClintock, W. E., Richard, E. C.: 2009, *Geophys. Res. Lett.* **36**, Issue 1, CiteID L01101.